Abstract Organic microcavities provide unique properties that are highly advantageous for designing microlasers, but lack in efficient ways to directly integrate electrodes able to drive high currents. The introduction of thin, patterned metal films, leading to the formation of local Tamm-plasmon-polariton states, has been recently demonstrated as a possible route to preserving coherence in the presence of significant optical loss. Here, periodic micron-scale gratings of silver are embedded into a high-quality organic microcavity, creating a crystal-like photonic potential structure. Despite strong absorption of metallic layers, these structures readily lase upon optical excitation. In that case, the above threshold emission originates not from isolate metal-free areas but instead from phase-locked supermodes spreading over several grating periods. Remarkably, in-plane coherence can spread even further when decreasing the grating period, covering distances of more than 50 µm and more than 10 metal stripes. One- and two-dimensional gratings with varying periods are investigated using tomographic scanning of the k-space emission fine structure, which exhibits a strong dependence on the grating geometry. These results support the fabrication of highly customizable organic microlasers with tailored in-plane coherence, and demonstrate the coexistence of extended coherence and optical loss.

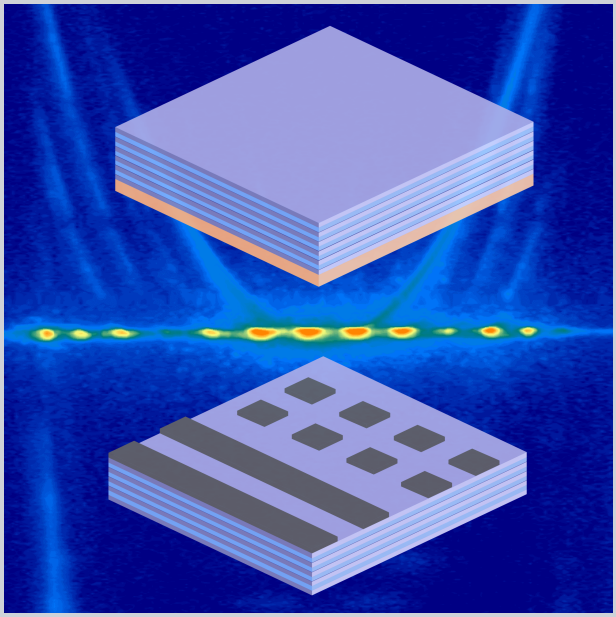

Phase-locked lasing in one- and two-dimensionally patterned metal-organic microcavities

Andreas Mischok[1,2,*], Mona Kliem[1], Robert Brückner[1], Stefan Meister[1], Hartmut Fröb[1], Malte C. Gather[2], Karl Leo[1]

1. Introduction

Organic microlasers promise a range of useful applications and are therefore of considerable interest in current research [1, 2]. However, the realization of an electrically pumped solid state organic laser remains elusive and is still regarded as the ”holy grail“ of the field. While considerable effort is directed towards highly efficient conductive as well as emissive organic materials [3] and polariton lasing [4–6], identifying efficient electrode designs is equally important. Most cavity designs for organic microlasers utilize either distributed feedback on a pre-structured grating or vertical feedback by sandwiching the active layer in between highly reflective distributed Bragg reflectors (DBRs) [7], with the latter having advantages in device footprint and offering surface emission. Such vertical microcavities efficiently confine light between the dielectric mirrors, leading to a parabolic dispersion of cavity photons, but usually do not offer a direct way of electrical contacting. By introducing thin, highly conductive metal films into such cavities, their photonic potential is altered. As cavity photons or polaritons interact with plasmons in the metal, they experience a jump in phase, leading to the creation of red-shifted states known as Tamm-plasmons-polaritons (TPPs) [8, 9] which have been shown to have the potential for high optical quality [10, 11]. In devices with extended metal layers, these have found a multitude of use for lasers [11, 12], thermal emitters [13], and exciton-polariton coupling [14, 15] as well as sensing and photodetection [16, 17]. Patterning this metal layer however, leads to a local shift in cavity potential [18] and enables strong lateral confinement [19–21], but also surprisingly facilitates a macroscopic in-plane coherence [22] where the coherent mode is spread across several periods of a metal grating. When coherent emission couples between individual spots of lasing or polariton condensates, their phases interlock [22–28] and complex supermodes are formed, exhibiting an intricate fine structure in real-, k-, and phase-space.

[1] Dresden Integrated Center for Applied Physics and Photonic Materials, Technische Universität Dresden, Nöthnitzer Strasse 61, 01187 Dresden, Germany [2] Organic Semiconductor Centre, SUPA, School of Physics and Astronomy, University of St. Andrews, North Haugh, St. Andrews KY16 9SS, UK
[*] Corresponding author: e-mail: am470@st-andrews.ac.uk

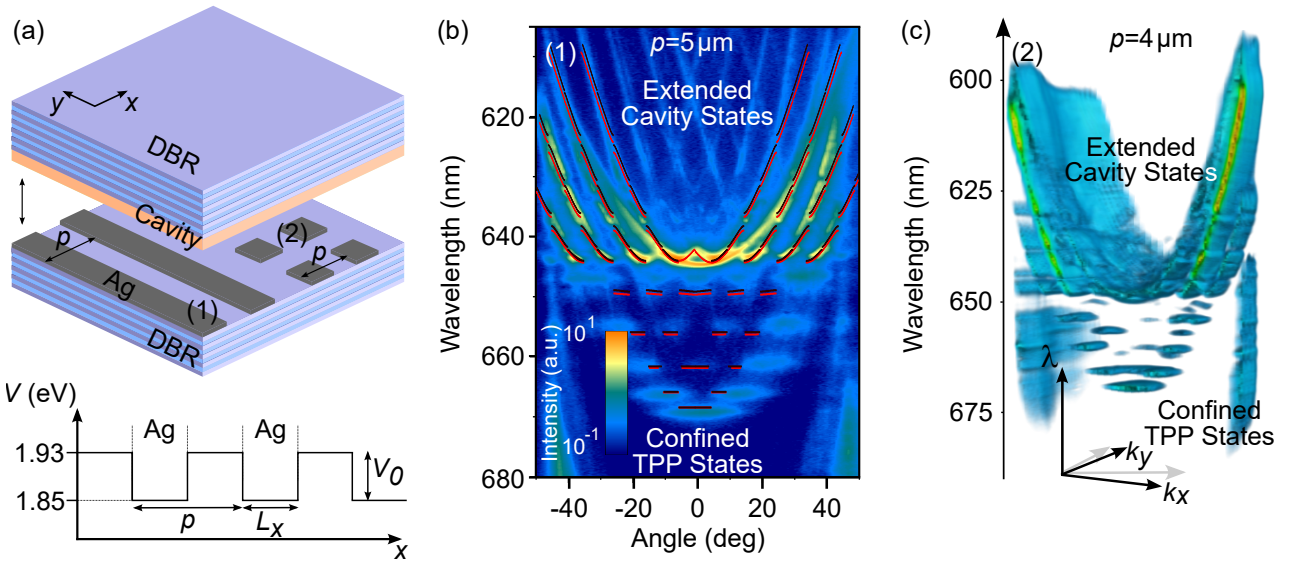

Figure 1 (a) Sample schematic of the microcavity with patterned metal layers. On top of the bottom DBR, a thin layer of silver is patterned to obtain either 1D stripe- (type (1)) or 2D dot- (type (2)) and hole- gratings. The lower part shows the photonic potential in the patterned microcavity, where potential wells are created at the position of the silver structures. (b) Dispersion of a stripe-grating microcavity red in k_x - direction. Introducing a 1D grating of type (1) (compare (a)), with a period of 5 µm leads to the formation of trapped discrete Tamm-plasmon-polariton (TPP) states (> 645 nm) and a Bloch-like band structure (< 645 nm). Bright (dark) red lines show the calculated band structure of the device in TE (TM) polarization. (c) Dispersion tomography of a dot-grating microcavity (type (2)) with a period of 4 µm, showcasing fully confined TPP states below and extended Bloch states above the potential barrier (at ≈ 645 nm).

Here, we introduce both one- and two-dimensional metal gratings into an organic microcavity and vary the period of these structures to systematically study the influence on above-threshold emission. In all cases, we observe lasing from phase-locked states spanning over many periods. Surprisingly, coherence is retained for various types of gratings, even when the majority of the sample surface is covered by metal. Utilizing dispersion tomography, we investigate the k-space fine structure of such phase-locked lasing modes for one- and two-dimensional gratings and find an enhanced spread of coherence compared to unpatterned devices.

2. Methods and Materials

The structure of the investigated device is schematically drawn in Figure 1 (a). The design comprises two DBRs with 10.5 alternating $\lambda/4$ layers of TiO_2 ($n \approx 2.15$) and SiO_2 ($n \approx 1.45$, raw materials purchased from Prof. Feierabend GmbH) sandwiching an organic active $\lambda/2$ layer of Tris-(8-hydroxyquinolinato)-aluminium (Alq_3, purchased from Sigma Aldrich) doped by 2 wt% with the laser dye Dicyanomethylene-2-methyl-6-p-dimethylaminostyryl-4H-pyran (DCM, purchased from Radiant laser dyes).

Between bottom DBR and organic cavity, a thin silver layer (≈ 30 nm) is deposited and patterned into (i) a one-dimensional periodic stripe grating (Fig. 1 (a), type (1)), (ii) a two-dimensional periodic square (Fig. 1 (a), type (2)) or (iii) hole grating with periods between 4 µm and 9 µm. The interaction between cavity photons and the plasmonic metal layer now leads to the formation of TPP states [8, 9], where the highest energy TPP state is significantly red-shifted compared to the original cavity mode. Consequently, patterning the silver film leads to the formation of photonic potential wells [18] as depicted in the lower half of Fig. 1 (a), which are the building blocks to create one- and two-dimensional lattices [29].

Here, the oxide layers are deposited via electron-beam evaporation in a custom vacuum chamber at a base pressure of 10^{-6} mbar and a partial oxygen pressure of 2×10^{-4} mbar to prevent the formation of sub-oxides. The organic materials are purified by vacuum gradient sublimation at least twice before they are deposited by thermal co-evaporation of matrix and dopant at a base pressure of 10^{-8} mbar. To facilitate the metallic structures of interest, a negative photoresist (AZ nLOF2020 from MicroChemicals) is patterned using a SUESS MJB4 mask aligner to act as lift-off resist before subsequently depositing a 30 nm thick layer of silver on top of an adhesion layer of 2 nm gold. After lift-off, the organic layer and top DBR are deposited on the final silver structures.

The devices are investigated using angle-resolved micro-photoluminescence spectroscopy, with a high NA objective (NA=0.8, 63×) projecting the Fourier plane of the sample emission onto the entrance slit of an 0.6 m spectrometer equipped with a cooled charge-coupled device. For sample excitation, either a cw laser diode at 405 nm (Coherent CUBE 405-50C) excites the matrix (Alq_3), to record spontaneous emission, or a pulsed 532 nm solid state laser (1.5 ns

pulse length at 2 kHz repetition, CryLas FDSS-532-Q2) excites the laser dye (DCM) directly and is used for both spontaneous and stimulated emission of the device.

For tomographic scanning along the k_y axis, the far field lens is moved out of the optical axis to record higher in-plane angles (details see [30]). The final image is recreated using Mayavi [31].

3. Results

3.1. Dispersion in One- and Two-Dimensional Gratings

Figure 1 (b) shows the k_x - dispersion of a $\lambda/2$ microcavity with 30 nm of silver patterned into stripes along the y-axis, with a period of 5 µm (type (1)). The one-dimensional photonic wires that are created by the silver stripes efficiently confine TPP states in red the observed x-direction [18] within potential wells of depth $V_0 = 80$ meV. This strong confinement results in discrete, flat modes in the dispersion, localized below the potential barrier at wavelengths greater than 645 nm. Above this barrier, photons travel freely between adjacent metal-free areas, exhibiting a Bloch-like band structure of the extended cavity states. To confirm our observation, we calculate the Bloch bands via a modified Kronig-Penney model [18, 32]. At $k_y = 0$, the cavity energy is given by:

$$E(k) = \hbar c\sqrt{k_z^2 + k_x^2} \approx E_0 + \frac{\hbar^2}{2m_{\text{phot}}}k_x^2, \qquad (1)$$

with $\hbar$ as the reduced Planck constant, c the speed of light in the organic material, $E_0 \approx \pi\hbar c/L_{\text{C}}$ the energy of the fundamental cavity mode, the cavity length L_{C}, and the effective mass of photons m_{phot}. In vertical microcavities, photons and polaritons obtain an effective mass due to the vertical confinement between the mirrors, its value being on the order of 10^{-5} times the free electron mass. When the cavity is detuned from the DBR design wavelength, as is inevitably the case in these metal-organic devices, this effective mass becomes dependent on the polarization of light. By considering cavity length and DBR penetration depth of the cavity photons [32, 33], we obtain values of $m_{\text{phot,TE}} = 1.06 \times 10^{-35}$ kg and $m_{\text{phot,TM}} = 1.02 \times 10^{-35}$ kg. The resulting values can be used to calculate the band structure of the well-known Kronig-Penney model corresponding to the artificial potential structure created here. In Fig. 1 (b), this calculation is overlaid on the measured dispersion as bright (dark) red lines, representing the calculated bands in TE (TM) polarization. Both discrete, core-electron-like states below the potential barrier (at ≈ 645 nm), as well as the extended, valence-electron-like bands above the barrier are well reproduced in the calculation. A further variation of periods in this structure is shown in the supporting information, Figure S1. While the dispersion perpendicular to the stripe orientation exhibits this rich structure, no confinement is observed in parallel direction red (data not shown here). As demonstrated previously for dielectric photonic wires embedded in such cavities [30], dispersion parabolas appear in k_y-direction, with additional parabolic branches for the corresponding discrete states at higher k_x.

It is also important to note that the confined TPP states exhibit broader linewidths and in turn lower quality factors (<450) when compared to the above-barrier Bloch bands (600 - 1000). As the TPPs are highly localized on the metal while the above-barrier states mainly reside in the metal-free area, it becomes clear that the parasitic absorption of this metal layer limits the cavity photon lifetime and thus the quality factor here.

By comparison to the one-dimensional structure, the two-dimensional square dot grating leads to a full confinement of light. Figure 1 (c) shows a reconstructed tomographic scan of the full dispersion in both k_x and k_y directions for such a device with a period of 4 µm. As light in TPP states is now essentially trapped at the position of a square metal dot, the dispersion exhibits fully flat discrete modes below the confining potential (again > 645 nm), in both k_x and k_y directions, according to [34]:

$$E(k) \approx \hbar c\sqrt{\frac{\pi}{L_{\text{C}}} + \frac{\pi}{L_x}(q_x+1) + \frac{\pi}{L_y}(q_y+1)}, \qquad (2)$$

with L_x, L_y and q_x, q_y as potential width and mode number in x and y-direction, respectively. Again, the behaviour above the barrier shows a Bloch-like band structure, now in two dimensions, albeit more difficult to resolve in the experiment.

Interestingly, the highest below-barrier states already show signs of cross-talk between different stripes, that is, they deviate from a completely flat dispersion and are able to travel in between different metal stripes without losing coherence. It is important to note that the observation of such a complex dispersion indicates the presence of a high degree of in-plane coherence in the spontaneous emission. This confirms the high quality of the cavity and the metal patterning.

A third type of patterning is also realized, namely the inverse of pattern type (2), i.e. a fully metal-covered bottom mirror with a square hole grating. For this structure, the dispersion is not fundamentally different from the dot pattern, although the degree of confinement in TPP states is naturally much lower. A clear difference with respect to the dot grating can be seen in their stimulated emission fine structure.

3.2. Stimulated Emission of Phase-Locked States

For increasing excitation pulse energy, all investigated systems show a clear nonlinear transition into stimulated emission, as shown in supporting information Figure S2. While in a typical, unpatterned microcavity, lasing originates from the apex of the dispersion parabola and extends isotropically in all in-plane directions with a radius of about 10 µm, the situation becomes much more complex in patterned systems.

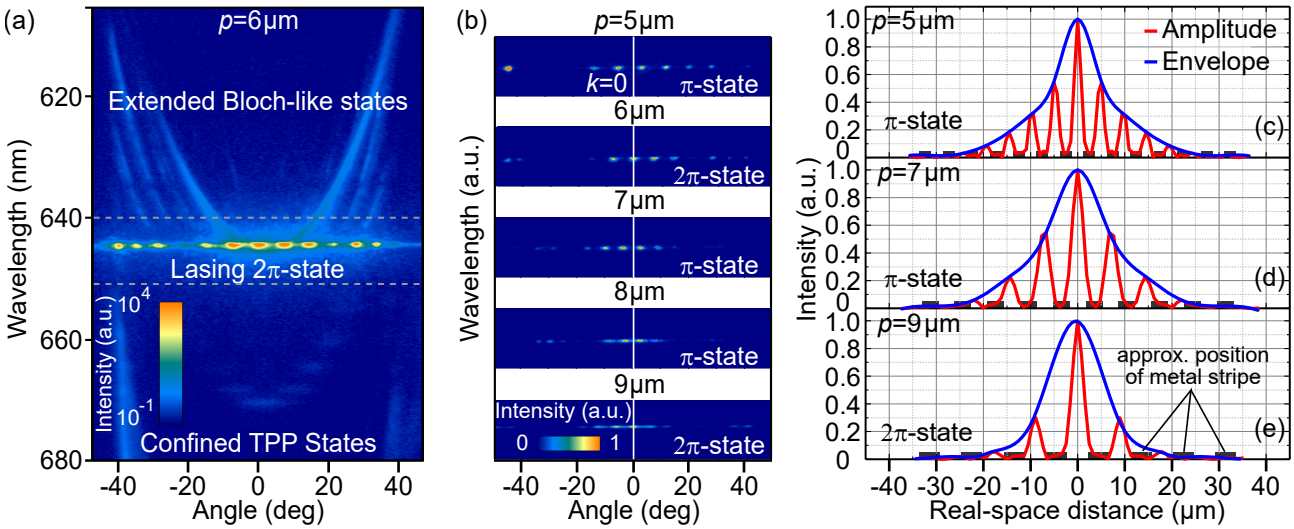

Figure 2 (a) Dispersion of a lasing 2π-state in a stripe-grating microcavity (type (1)) at $p = 6.0\,\mu$m. Due to the modified photonic potential, lasing starts as a supermode spanning several periods. (b) Lasing states at varying periods. By decreasing the period from 9 µm to 5 µm, the k-space separation of lasing antinodes increases while their individual width decreases - pointing towards a larger spread of coherence in real space. Please note that the color scale in (b) is linear while it is logarithmic in (a). (c)-(e) Real-space distribution of coherent emission. By Fourier-transformation of the far-field image, the coherent spatial extension of lasing states can be obtained. In each case, the lasing supermode is spread over several stripe periods, confirming the long-range coherence of the emission. For smaller periods (compare $p = 5\,\mu$m (c), 7 µm (d), 9 µm (e)) the mode extension increases both in number of periods as well as in absolute distance.

While some systems show lasing from single confined regions created by patterning [12,21,22], in our system lasing always originates from a phase-locked supermode spanning a multitude of grating periods. Despite apparent optical loss induced by the silver structure, such an extended mode is consistently preferred over uncoupled lasing from individual stripes. In the investigated patterns, the supermode stretches over in-plane distances of tens of µm, and covers up to ∼10 grating periods.

Figure 2 (a) shows the dispersion of a lasing cavity with a type (1) stripe-grating at a grating period of $p = 6\,\mu$m when excited in the centre of a metal-free stripe with a spot diameter of 5 µm. The emission of the device is concentrated around a number of evenly spaced spots at a wavelength of 644 nm and an angular spacing of $\approx 7.5^\circ$. This lasing mode can be identified as the 2π-state [18, 22, 35] in the lowest band of the Bloch-like dispersion above the energy barrier [28]. The spacing of lasing spots corresponds to the grating period and all spots are part of the same coherent mode, showing the same threshold behaviour. A trend of increased spacing of lasing spots in devices with different grating periods can be clearly seen in Figure 2 (b), where the period is varied from $p = 9\,\mu$m (lowest image) to $p = 5\,\mu$m (highest image), as the spacing in reciprocal space follows the inverse of the grating period, according to the angle difference $\Delta\vartheta = \sin^{-1}\lambda_c/p$, with the fundamental cavity wavelength λ_c. Two features become immediately obvious in this picture: First, the parity of the lasing states changes between π and 2π for varying periods. As an increasing period means also an increase in the width of the TPP-confining potential well, the number of trapped modes varies between different gratings. As we have shown before, the emergence of π and 2π states depends on the parity of the lowest-energy Bloch band [18]. In turn, this depends on the parity of the highest-energy discrete state and thus their total number, i.e. the lasing state switches from π for an uneven, to 2π for an even number of discrete states. Second, the width of the individual spots in k-space decreases for a decreasing grating period. In turn, the real space extension of the lasing mode increases for smaller periods and spans not only a single stripe but a multitude of phase-locked lasing spots in adjacent metal-free areas [22].

To confirm our observation, we perform a Fourier-transform of the wavelength-integrated emission in k-space. This way, the true extension of the coherent mode can be obtained. Figure 2 (c)-(e) shows the resulting intensity profiles along the x-direction for grating periods of 5 µm (c), 7 µm (d), and 9 µm (e), respectively. Indeed this analysis confirms the increased spread of the coherent mode over large in-plane distances. It is interesting to note that for a smaller grating period, the coherent mode not only encompasses a larger number of periods, but also increases in absolute size. Judging from the amplitude of the Fourier transform for $p = 5\,\mu$m, we observe a spread of coherence over at least 50 µm and 10 periods of the metal grating. It turns out that the inclusion of such a lossy grating does not diminish in-plane coherence, but instead even enhances it for smaller periods. This observation agrees with similar results we have obtained earlier on microcavities deposited on a periodically patterned substrate [36]. In the present study, even the additional parasitic absorption introduced by an intracavity metal layer is compatible with a large degree of coherence and suggests the possibility of integrating highly conductive electrodes in high-quality cavities.

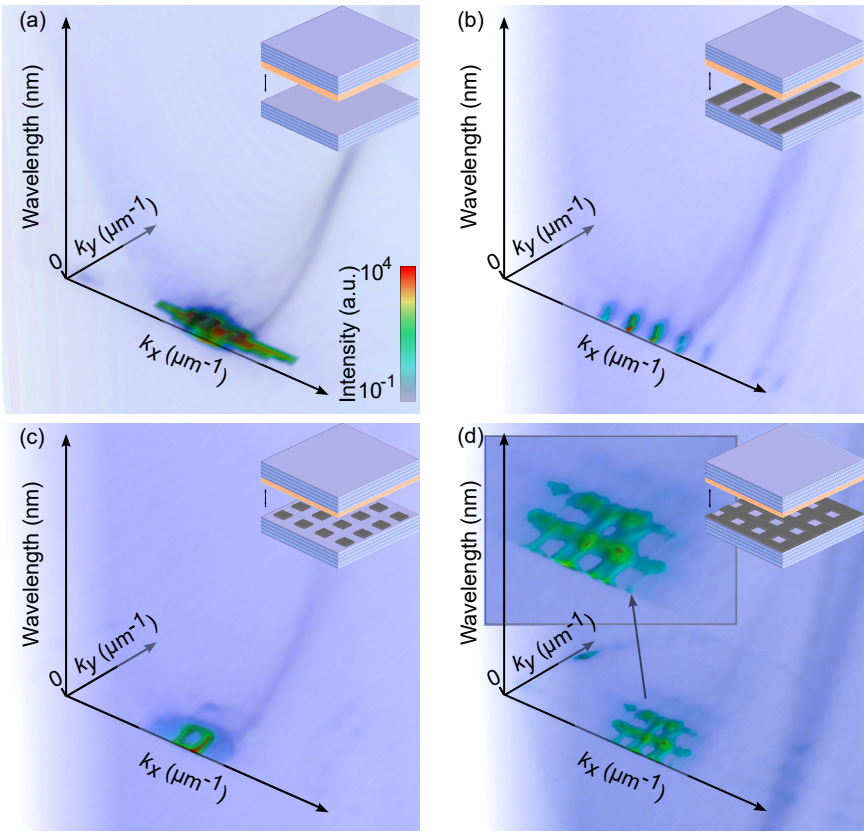

Figure 3 Dispersion tomography of lasing in (a) an unpatterned cavity, (b) a stripe-grating cavity at $p = 7\,\mu$m, (c) a dot-grating at $p = 7\,\mu$m, and (d) a hole-grating at $p = 8\,\mu$m (compare with sketches as inset). The characteristics of the grating employed are manifested in the coherent k-space emission of the corresponding microcavity as well. In turn, coherence in real space is spread according to the Fourier-transformation of the laser modes observed here i.e. uniformly (a), mainly in x-direction (b), or in x- and y- directions ((c),(d)).

3.3. Dispersion Tomography of Phase-Locked Lasing Modes

As a final step, stimulated emission is also assessed in the two-dimensional gratings of metal dots and holes introduced earlier. To obtain a full picture of the coherent mode, the dispersion in k_x-direction is recorded while tomographically scanning the k_y-direction by moving the Fourier-imaging lens out of the optical axis [30]. Figure 3 shows the recreated three-dimensional tomograms of stimulated emission comparing an unpatterned laser (a) and devices with a stripe grating at $p = 7\,\mu$m (b), a metal dot grating at $p = 7\,\mu$m (c), and a hole grating at $p = 8\,\mu$m (d). For the unpatterned cavity and the stripe-grating, the mode is not confined in k_y direction and thus shows a large width in k space. In k_x direction, however, the difference between the two becomes most striking. The mode of the unpatterned laser covers at least five of the individual spots observed in the stripe grating, suggesting an inverse behaviour in real space. In the two-dimensional gratings, the k space dispersion behaves according to the Fourier transform of the actual grating, suggesting that emission is concentrated at the corners of metal dots for grating type (2), Fig. 3 (c), and inside the metal-free holes for the inverse grating as seen in Fig. 3 (d) (compare schematic 2-D FFT in supporting information, Fig. S3). In both cases, the observed mode fine structure points toward an increased in-plane spread of coherence in two dimensions. Even for a comparatively large aspect ratio of metal-covered to metal-free areas as in Fig. 3 (d), macroscopically coherent emission is obtained in these organic microcavities. This effect should allow designing effective electrodes for electrically driven solid state organic microlasers.

4. Conclusion

We have demonstrated how the incorporation of a highly-conductive silver layer into an organic microcavity is compatible with laser emission and how a micro-structure of said metal can even aid in spreading in-plane coherence. By patterning gratings with periods of few micrometers, optical losses are minimized while at the same time providing an efficient electrical contacting in future devices. Due to the coupling of emission over several grating periods, we observe the formation of a photonic band structure and phase-locked lasing in such systems with coherent emission extending over 10 periods of metal grating and a lower limit of 50 μm in the sample plane. Furthermore, we demonstrate the shaping of the laser mode in two-dimensional hole and dot gratings, exhibiting a distinct fine structure as dictated by the metal patterning. Coherent emission persists even when the majority of the area is covered in silver. We are confident that our results will aid both in controlled laser mode shaping as well as electrode design for electrically driven organic solid state lasers.

Acknowledgements

The authors gratefully acknowledge financial support by the Deutsche Forschungsgemeinschaft, Projects No. LE 747/53-1 and LE 747/55-1, and via the excellence cluster cfaed. A.M. and M.C.G. acknowledge additional funding by the Volkswagen-Stiftung, Project No. A123031. K.L. acknowledges support by the Canadian Institute for Advanced Research (CIFAR).

Supporting Information

Supporting information containing additional dispersion measurements, input-output measurements, as well as fast Fourier transformation images are available. In addition, supporting movies 1-5 show rotating animations of Fig. 1 (c) and Fig. 3 (a)-(d).

Key words: organic microlaser, Tamm plasmon polariton, phase locked lasing, metal-organic microcavity, photonic lattices

References

[1] S. Chénais and S. Forget, "Recent advances in solid-state organic lasers," *Polymer International*, vol. 61, no. 3, pp. 390–406, 2012.

[2] A. J. Kuehne and M. C. Gather, "Organic lasers: recent developments on materials, device geometries, and fabrication techniques," *Chemical Reviews*, vol. 116, no. 21, pp. 12823–12864, 2016.

[3] J. Liu, H. Zhang, H. Dong, L. Meng, L. Jiang, L. Jiang, Y. Wang, J. Yu, Y. Sun, W. Hu, and A. J. Heeger, "High mobility emissive organic semiconductor," *Nature Communications*, vol. 6, p. 10032, 2015.

[4] K. Daskalakis, S. Maier, R. Murray, and S. Kéna-Cohen, "Nonlinear interactions in an organic polariton condensate," *Nature Materials*, vol. 13, no. 3, pp. 271–278, 2014.

[5] J. D. Plumhof, T. Stöferle, L. Mai, U. Scherf, and R. F. Mahrt, "Room-temperature bose–einstein condensation of cavity exciton–polaritons in a polymer," *Nature Materials*, vol. 13, no. 3, pp. 247–252, 2014.

[6] C. P. Dietrich, A. Steude, L. Tropf, M. Schubert, N. M. Kronenberg, K. Ostermann, S. Höfling, and M. C. Gather, "An exciton-polariton laser based on biologically produced fluorescent protein," *Science Advances*, vol. 2, no. 8, p. e1600666, 2016.

[7] K. J. Vahala, "Optical microcavities," *Nature*, vol. 424, no. 6950, pp. 839–846, 2003.

[8] M. Kaliteevski, I. Iorsh, S. Brand, R. Abram, J. Chamberlain, A. Kavokin, and I. Shelykh, "Tamm plasmon-polaritons: Possible electromagnetic states at the interface of a metal and a dielectric Bragg mirror," *Physical Review B*, vol. 76, no. 16, p. 165415, 2007.

[9] R. Brückner, M. Sudzius, S. Hintschich, H. Fröb, V. Lyssenko, and K. Leo, "Hybrid optical Tamm states in a planar dielectric microcavity," *Physical Review B*, vol. 83, no. 3, p. 033405, 2011.

[10] C. Symonds, S. Azzini, G. Lheureux, A. Piednoir, J. Benoit, A. Lemaitre, P. Senellart, and J. Bellessa, "High quality factor confined tamm modes," *Scientific Reports*, vol. 7, no. 1, p. 3859, 2017.

[11] R. Brückner, V. Lyssenko, S. Hofmann, and K. Leo, "Lasing of Tamm states in highly efficient organic devices based on small-molecule organic semiconductors," *Faraday Discussions*, vol. 174, pp. 183–201, 2014.

[12] C. Symonds, G. Lheureux, J. Hugonin, J. Greffet, J. Laverdant, G. Brucoli, A. Lemaitre, P. Senellart, and J. Bellessa, "Confined Tamm plasmon lasers," *Nano Letters*, vol. 13, no. 7, pp. 3179–3184, 2013.

[13] Z.-Y. Yang, S. Ishii, T. Yokoyama, T. D. Dao, M.-G. Sun, P. S. Pankin, I. V. Timofeev, T. Nagao, and K.-P. Chen, "Narrowband wavelength selective thermal emitters by confined tamm plasmon polaritons," *ACS Photonics*, vol. 4, no. 9, pp. 2212–2219, 2017.

[14] M. Wurdack, N. Lundt, M. Klaas, V. Baumann, A. V. Kavokin, S. Höfling, and C. Schneider, "Observation of hybrid Tamm-plasmon exciton-polaritons with GaAs quantum wells and a MoSe 2 monolayer," *Nature Communications*, vol. 8, no. 1, p. 259, 2017.

[15] C. Grossmann, C. Coulson, G. Christmann, I. Farrer, H. Beere, D. Ritchie, and J. Baumberg, "Tuneable polaritonics at room temperature with strongly coupled tamm plasmon polaritons in metal/air-gap microcavities," *Applied Physics Letters*, vol. 98, no. 23, p. 231105, 2011.

[16] C. Zhang, K. Wu, V. Giannini, and X. Li, "Planar hot-electron photodetection with tamm plasmons," *ACS Nano*, vol. 11, no. 2, pp. 1719–1727, 2017.

[17] A. Mischok, B. Siegmund, D. S. Ghosh, J. Benduhn, D. Spoltore, M. Bohm, H. Frob, C. Korner, K. Leo, and K. Vandewal, "Controlling tamm plasmons for organic narrowband near-infrared photodetectors," *ACS Photonics*, vol. 4, no. 9, pp. 2228–2234, 2017.

[18] A. Mischok, V. G. Lyssenko, R. Brückner, F. Löchner, R. Scholz, A. A. Zakhidov, H. Fröb, and K. Leo, "Zero-and π-states in a periodic array of deep photonic wires," *Advanced Optical Materials*, vol. 2, no. 8, pp. 746–750, 2014.

[19] O. Gazzano, S. M. de Vasconcellos, K. Gauthron, C. Symonds, J. Bloch, P. Voisin, J. Bellessa, A. Lemaître, and P. Senellart, "Evidence for confined tamm plasmon modes under metallic microdisks and application to the control of spontaneous optical emission," *Physical Review Letters*, vol. 107, no. 24, p. 247402, 2011.

[20] I. Y. Chestnov, E. Sedov, S. Kutrovskaya, A. Kucherik, S. Arakelian, and A. Kavokin, "One-dimensional tamm plasmons: Spatial confinement, propagation, and polarization properties," *Physical Review B*, vol. 96, no. 24, p. 245309, 2017.

[21] A. Mischok, R. Brückner, M. Sudzius, C. Reinhardt, V. G. Lyssenko, H. Fröb, and K. Leo, "Photonic confinement in laterally structured metal-organic microcavities," *Applied Physics Letters*, vol. 105, no. 5, p. 051108, 2014.

[22] R. Brückner, A. A. Zakhidov, R. Scholz, M. Sudzius, S. Hintschich, H. Fröb, V. Lyssenko, and K. Leo, "Phase-locked coherent modes in a patterned metal-organic microcavity," *Nature Photonics*, vol. 6, no. 5, pp. 322–326, 2012.

[23] H. Ohadi, R. Gregory, T. Freegarde, Y. Rubo, A. Kavokin, N. G. Berloff, and P. Lagoudakis, "Nontrivial phase coupling in polariton multiplets," *Physical Review X*, vol. 6, no. 3, p. 031032, 2016.

[24] E. Tan, H. Sigurdsson, and T. Liew, "Parity bifurcations in trapped multistable phase locked exciton-polariton condensates," *arXiv preprint arXiv:1712.02559*, 2017.
[25] A. J. Kollár, A. T. Papageorge, V. D. Vaidya, Y. Guo, J. Keeling, and B. L. Lev, "Supermode-density-wave-polariton condensation with a bose–einstein condensate in a multimode cavity," *Nature Communications*, vol. 8, 2017.
[26] G. Christmann, G. Tosi, N. G. Berloff, P. Tsotsis, P. S. Eldridge, Z. Hatzopoulos, P. G. Savvidis, and J. J. Baumberg, "Oscillatory solitons and time-resolved phase locking of two polariton condensates," *New Journal of Physics*, vol. 16, no. 10, p. 103039, 2014.
[27] T. Gao, E. Estrecho, G. Li, O. Egorov, X. Ma, K. Winkler, M. Kamp, C. Schneider, S. Hoefling, A. Truscott, and E. A. Ostrovskaya, "Talbot effect for exciton polaritons," *Physical Review Letters*, vol. 117, no. 9, p. 097403, 2016.
[28] A. Nalitov, T. C. H. Liew, A. Kavokin, B. Altshuler, and Y. Rubo, "Spontaneous polariton currents in periodic lateral chains," *Physical review letters*, vol. 119, no. 6, p. 067406, 2017.
[29] K. Winkler, J. Fischer, A. Schade, M. Amthor, R. Dall, J. Geßler, M. Emmerling, E. A. Ostrovskaya, M. Kamp, C. Schneider, and S. Höfling, "A polariton condensate in a photonic crystal potential landscape," *New Journal of Physics*, vol. 17, no. 2, p. 023001, 2015.
[30] A. Mischok, F. Lemke, C. Reinhardt, R. Brückner, A. Zakhidov, S. Hintschich, H. Fröb, V. Lyssenko, and K. Leo, "Dispersion tomography of an organic photonic-wire microcavity," *Applied Physics Letters*, vol. 103, no. 18, p. 183302, 2013.
[31] P. Ramachandran and G. Varoquaux, "Mayavi: 3d visualization of scientific data," *Computing in Science & Engineering*, vol. 13, no. 2, pp. 40–51, 2011.
[32] F. J. Löchner, A. Mischok, R. Brückner, V. G. Lyssenko, A. A. Zakhidov, H. Fröb, and K. Leo, "Coexisting localized and extended optical Bloch states in a periodic deep wire array microcavity," *Superlattices and Microstructures*, vol. 85, pp. 646–652, 2015.
[33] G. Panzarini, L. C. Andreani, A. Armitage, D. Baxter, M. Skolnick, V. Astratov, J. Roberts, A. V. Kavokin, M. R. Vladimirova, and M. Kaliteevski, "Exciton-light coupling in single and coupled semiconductor microcavities: Polariton dispersion and polarization splitting," *Physical Review B*, vol. 59, no. 7, p. 5082, 1999.
[34] T. Gutbrod, M. Bayer, A. Forchel, P. A. Knipp, T. L. Reinecke, A. Tartakovskii, V. D. Kulakovskii, N. A. Gippius, and S. G. Tikhodeev, "Angle dependence of the spontaneous emission from confined optical modes in photonic dots," *Physical Review B*, vol. 59, pp. 2223–2229, Jan 1999.
[35] C. W. Lai, N. Y. Kim, S. Utsunomiya, G. Roumpos, H. Deng, M. D. Fraser, T. Byrnes, P. Recher, N. Kumada, T. Fujisawa, and Y. Yamamoto, "Coherent zero-state and π-state in an exciton-polariton condensate array," *Nature*, vol. 450, no. 7169, 2007.
[36] A. Mischok, T. Wagner, R. Brückner, M. Sudzius, H. Fröb, V. G. Lyssenko, and K. Leo, "Lasing and macroscopic coherence of hybridized modes in coupled 2d waveguide-vcsel resonators," *Advanced Optical Materials*, vol. 4, no. 8, pp. 1215–1221, 2016.